Evolution of Fractal Patterns during a Classical-Quantum Transition

A. P. Micolich,[1] R. P. Taylor,[1,*] A. G. Davies,[2] J. P. Bird,[3] R. Newbury,[4] T. M. Fromhold,[5] A. Ehlert,[4] H. Linke,[1] L. D. Macks,[2] W. R. Tribe,[2] E. H. Linfield,[2] D. A. Ritchie,[2] J. Cooper,[6] Y. Aoyagi,[6] and P. B. Wilkinson[5]

[1]*Materials Science Institute, Physics Department, University of Oregon, Eugene, Oregon 97403-1274*
[2]*Cavendish Laboratory, University of Cambridge, Madingley Road, Cambridge CB3 0HE, United Kingdom*
[3]*Center for Solid State Research, Arizona State University, Tempe, Arizona 85287-6206*
[4]*School of Physics, University of New South Wales, Sydney, NSW 2052, Australia*
[5]*School of Physics and Astronomy, University of Nottingham, Nottingham NG7 2RD, United Kingdom*
[6]*Semiconductor Laboratory, RIKEN, 2-1 Hirosawa, Wako-shi, Saitama 351-0198, Japan*

(Received 14 December 2000; published 29 June 2001)

We investigate how fractals evolve into nonfractal behavior as the generation process is gradually suppressed. Fractals observed in the conductance of semiconductor billiards are of particular interest because the generation process is semiclassical and can be suppressed by transitions towards either fully classical or fully quantum-mechanical conduction. Investigating a range of billiards, we identify a "universal" behavior in the changeover from fractal to nonfractal conductance, which is described by a smooth evolution rather than deterioration in the fractal scaling properties.

DOI: 10.1103/PhysRevLett.87.036802 PACS numbers: 73.23.–b, 05.45.Df, 85.35.–p

Since fractals were first introduced to quantify the recurrence of structure at increasingly fine magnifications [1], they have successfully described a remarkable range of natural patterns [2]. However, many studies of fractals are "passive," where rather than actively interacting with the process generating the fractals, the experiments are limited to a simple monitoring role. A more powerful approach is to induce fractals in an artificially constructed system where the conditions can be controlled and adjusted with precision. To do this we construct micron-sized "billiards" in high quality semiconductor materials. Analogous to a billiard table, electrons move along a two-dimensional plane bounded by shaped walls. The distance ℓ between scattering sites within the semiconductor material is greater than that between the walls, and hence electrons passing between the billiard entrance and exit openings follow ballistic trajectories determined predominantly by the shape of the walls [3]. Electrons in the billiards follow both chaotic and stable classical trajectories and, through a semiclassical electron-wave interference process, the mixed stable-chaotic dynamics generate fractal patterns in the electrical conductance [4–11]. In this Letter, we investigate a fundamental question—how do fractals evolve into nonfractal behavior as the generating process is gradually suppressed? We suppress the semiclassical process using controlled transitions towards either fully classical or fully quantum-mechanical conduction. We show that the fractals are remarkably robust to the suppression process—the transition to nonfractal behavior is characterized by a smooth change in the fractal dimension rather than a reduction in the range of scales over which fractal behavior is observed.

The billiard construction technique [3,12] is shown in Fig. 1. Within the semiconductor heterostructure, a two-dimensional sheet of electrons is located at the interface between the lowest GaAs and AlGaAs layers. The billiard is defined in this sheet using patterned metallic gates (light gray) deposited on the heterostructure surface. A negative gate bias V_g defines tunable depletion regions (medium gray) that form the billiard walls in the sections of the electron sheet directly below the gates. This electrostatic technique produces a two-dimensional potential well with walls that have an approximately parabolic energy profile [4] (see Fig. 1, top right). These "soft-wall" billiards are predicted to generate mixed electron dynamics [4–7]. Table I summarizes the experimental parameters for the seven billiards investigated—the area A enclosed by the billiard, the number of quantized conducting modes n in the openings [3], the mean free path ℓ, and the temperature T at which the billiard is measured. We begin by considering a typical billiard (device e). Cooling the billiard reduces phase-breaking scattering events and the quantum-mechanical wave properties of the electrons become important. At $T = 0.03$ K, the characteristic phase coherence length is 33 times longer than the billiard width of 1 μm, ensuring that a typical electron maintains coherence while traversing the billiard. The ratio S of the billiard width to the electron Fermi wavelength ($\sim$40 nm) is sufficiently large that electron transport within the billiard is semiclassical rather than fully quantum mechanical. Within a semiclassical picture, the electron waves accumulate phase as they move along the trajectories and this determines the wave interference between pairs of trajectories that form closed loops [8]. We vary the phase, and hence the interference, by applying a small magnetic field B perpendicular to the plane of the billiard [3]. The resulting fluctuations in the magnetoconductance $G(B)$ are sensitive to the precise distribution of loop areas in the billiard [3,9–11]. For soft-wall billiards, the trajectory loop areas are expected to follow a power-law distribution [4–7]. This has been predicted [5] to produce fractal conductance fluctuations (FCF)—a

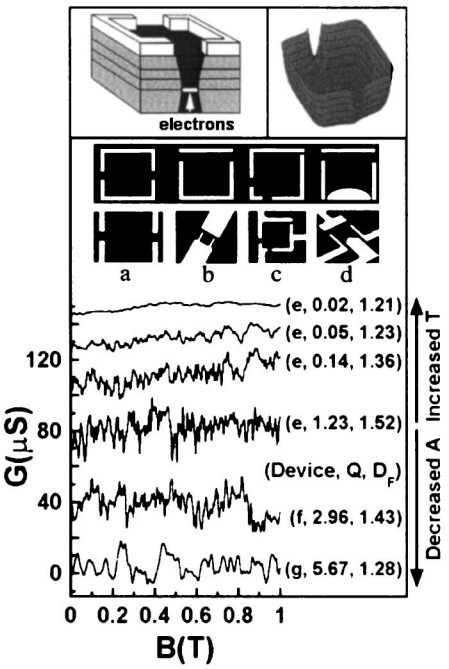

FIG. 1. Top left: A schematic representation of the billiard. The layers from surface down are n-GaAs, n-AlGaAs, AlGaAs, and GaAs. Top right: A simulation of a billiard's "soft-wall" potential profile where the potential energy (vertical) is plotted as a function of physical location in the billiard. Middle: Schematics of the gate patterns (not to scale) together with the equivalent scanning electron micrographs for four (a, b, c, and d) of the seven billiards investigated. The lithographic dimensions (vertical $\times$ horizontal) are a 30 $\times$ 2 μm, b 2 $\times$ 2 μm, c 1 $\times$ 1 μm, and d 0.6 $\times$ 0.7 μm. All billiard openings are 0.2 μm wide. Billiards e, f, and g have the same geometry as b but are different sizes (see Table I). Bottom: Magnetoconductance fluctuations measured for billiards e, f, and g (see trace labels) with $n = 2$ and $\ell = 4.4$ μm. From top to bottom the (T, A) values for the traces are (4.2 K, 1.0 μm^2), (1.4 K, 1.0 μm^2), (0.48 K, 1.0 μm^2), (0.03 K, 1.0 μm^2), (0.03 K, 0.36 μm^2), and (0.03 K, 0.16 μm^2). The right-hand brackets indicate (device, Q, D_F) (see text for definitions of Q and D_F). The traces are offset vertically for clarity.

fractal scaling of magnetoconductance fluctuation patterns at increasingly fine magnetic field scales — and FCF have since been observed [9–11].

Such fluctuations are clearly visible in the fourth (from top) trace of Fig. 1. This $G(B)$ trace is measured for device e at $T = 0.03$ K, where the conduction *within* the billiard is in the semiclassical regime (the implications of the low n value in the openings are discussed later). We emphasize that the fluctuations are reproducible and are *not* generated by measurement noise. The trace exhibits fluctuations on many magnetic field scales, indicating the *potential* for fractal scaling. The remaining traces in Fig. 1 demonstrate the effect of varying T and A. An increase in T reduces the electron phase coherence length and is therefore expected to induce more classical conduction. In contrast, a decrease in A reduces S and should therefore increase the importance of purely quantum-mechanical transport processes. It is clear from Fig. 1 that the complexity of the fluctuations decreases by increasing T (moving to the upper traces) or reducing A (moving to the lower traces obtained from the smaller billiards f and g). This suggests that deviations from semiclassical conduction within the billiard induce a profound change in the scaling properties of the fluctuations.

To quantify this change, we employ a fractal detection method known as the box-counting technique [1,2] where the $G(B)$ trace is covered with a computer-generated mesh of identical squares. The fractal dimension D_F quantifies the scaling relationship between patterns observed at different magnifications [1,2]. D_F is obtained by calculating the number of occupied squares in the mesh $N(\Delta B)$ as a function of square size ΔB. For fractal behavior [1,2], $N(\Delta B)$ scales according to $N(\Delta B) \sim \Delta B^{-D_F}$, where $1 < D_F < 2$. Therefore, by constructing a scaling plot of $\log N(\Delta B)$ against $\log \Delta B$, fractal behavior is detected as a straight line and quantified by extracting D_F from the gradient. Figure 2 shows a typical scaling plot. The dashed straight line is a guide to the eye, indicating that the data follow the fractal scaling relationship over the range $0.35 < \Delta B < 45$ mT. The values of the upper and lower "cutoffs," ΔB_2 and ΔB_3, are determined using the derivative plots shown in insets 2(a) and 2(b). ΔB_1 represents the measurement resolution limit of 0.1 mT. The data remain nonfractal up to ΔB_2 due to the dominance of measurement noise over signal for these small fluctuations in $G(B)$. ΔB_4 represents the length of the data trace, which is limited to $B < 150$ mT due to the emergence at higher fields of conduction processes that do not generate FCF

TABLE I. A summary of the billiard parameters discussed in the text. To investigate a large range of A values, we construct billiards with different physical areas. Tuning V_g is also used to change A. In particular, the bottom "plunger" gate featured in billiard d (see Fig. 1) can reduce A to less than 20% of the physical area enclosed by the gates. The opening widths and hence n are also reduced by increasing V_g. We vary ℓ by constructing billiards using different quality materials. Measurements are performed for a range of T. See the text for the definition of τ_q and Q.

Device	A (μm^2)	T (K)	ℓ (μm)	n	τ_q (ps)	Q
a	60.0	0.03	25	4	16.6	0.003
b	4.0	0.03	4.4	2	109.6	0.30
c	1.0	0.03–4.2	12	2–6	2.8–182.9	0.012–1.99
d	0.22–0.09	0.03	5.5	2	75.0–87.9	4.34–9.05
e	1.0	0.03–4.2	4.4	2	24.9–113.2	0.02–1.23
f	0.36	0.03–2.5	4.4	2	20.1–98.7	0.08–2.96
g	0.16	0.03	4.4	2	83.4	5.67

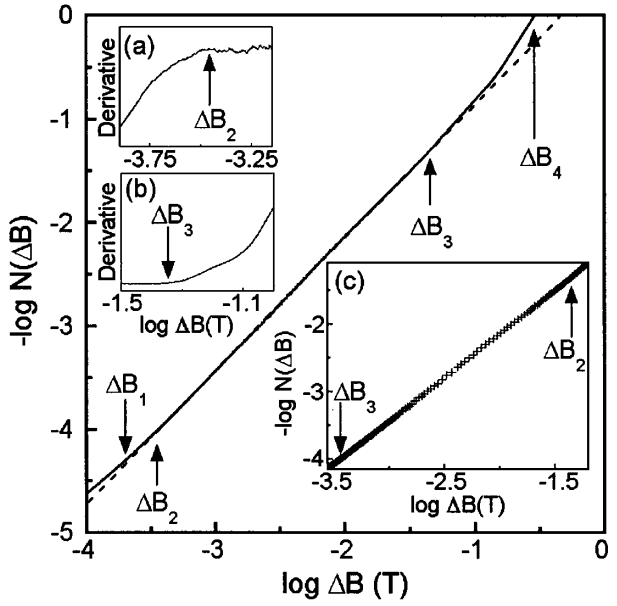

FIG. 2. The data (solid line) follow a straight line (dashed line) between the magnetic field scales ΔB_2 and ΔB_3. The insets (a) and (b) are derivative plots of the data and (c) shows the individual data points (for clarity only every tenth point is plotted).

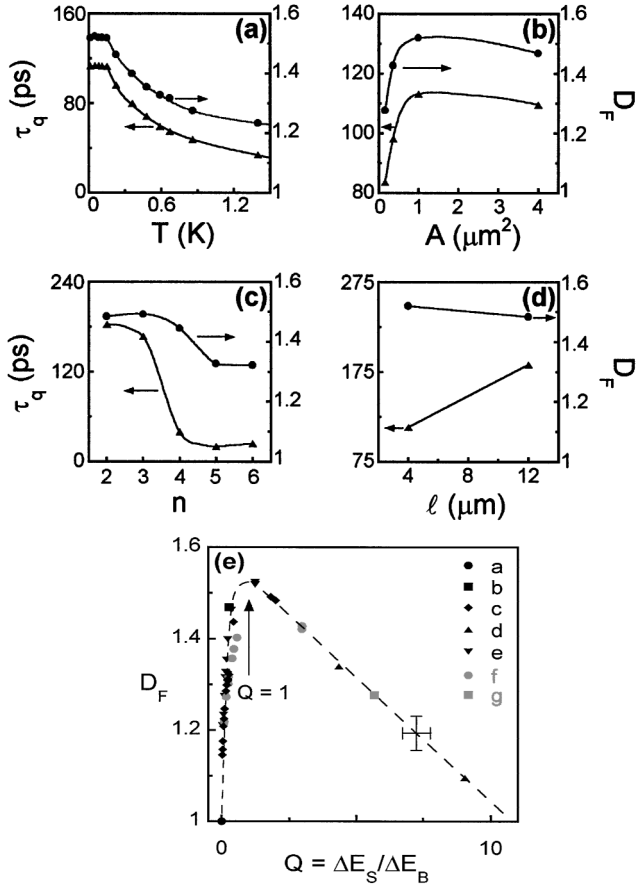

FIG. 3. In (a)–(d), τ_q and D_F are plotted against T, A, n, and ℓ. The τ_q values (triangles) are plotted along the left vertical axis while the D_F values (circles) are plotted along the right vertical axis. T, A, n, and ℓ are plotted along the horizontal axis for (a)–(d), respectively, with $A = 1\ \mu\text{m}^2, n = 2, \ell = 4.4\ \mu\text{m}$ in (a); $T = 30$ mK, $n = 2, \ell = 4.4\ \mu$m in (b); $T = 30$ mK, $A = 1\ \mu\text{m}^2, \ell = 4.4\ \mu$m in (c), and $T = 30$ mK, $A = 1\ \mu\text{m}^2, n = 2$ in (d). In (e), D_F is plotted against Q. The lines joining the data are guides to the eye. The error bars correspond to the *maximum* possible uncertainties in D_F and Q.

[10]. The upper cutoff occurs at a lower field scale ΔB_3 because it is necessary to fit at least 49 squares in the mesh in order to achieve sufficient box-counting statistics to resolve the fractal behavior. Inset 2(c) shows the individual data points within the fractal scaling range. To produce this plot we employ two refinements to the box-counting method—the variation method (where the data point density increases as small ΔB) and the horizontal structured elements method (where the density increases at large ΔB) [13]. Combining these two methods, we achieve a high data point density across all ΔB values, ensuring a reliable detection of fractal scaling.

Returning to Fig. 1, we use D_F to investigate the FCF evolution during the transition from classical to quantum-mechanical conduction. As T and A are adjusted to suppress the semiclassical process, the most anticipated scenario for the evolution of FCF towards a nonfractal trace is that the value of D_F remains constant while the range of ΔB over which fractal behavior is observed decreases to zero [14]. Instead, Fig. 1 reveals a more remarkable behavior where the value of D_F decreases *gradually* towards the nonfractal value of 1 in both the classical and quantum limits. We now consider *all* four adjustable experimental parameters (T, A, n, and ℓ) for the seven billiards presented in Fig. 1 and Table I. As demonstrated in Figs. 3(a)–3(d), the plots of D_F (circles) versus T, A, n, and ℓ all have different forms. However, we find that D_F changes in a *universal* way when plotted against a more general parameter Q that quantifies the transition towards resolvable, quantized energy levels within the billiard. We define Q as the ratio of the average energy level spacing ΔE_S to the average energy broadening ΔE_B. The condition $Q = 0$ corresponds to $\Delta E_S = 0$ or $\Delta E_B = \infty$. Q is increased either by increasing ΔE_S or decreasing ΔE_B, improving the resolution of the discrete energy levels. We calculate ΔE_S by dividing the energy of the highest occupied level by the total number of occupied energy levels and this equals $2\pi\hbar^2/m^*A$ (where m^* is the electron effective mass) [15]. ΔE_B is given by the quadrature summation of the billiard's two characteristic energy broadening widths—thermal broadening kT and the intrinsic energy level broadening $\hbar/\tau_q$ originating from phase-breaking scattering events that limit the lifetime τ_q of the quantum states [16]. Thus

$$Q = \frac{\Delta E_S}{\Delta E_B} = \frac{(2\pi\hbar^2)/(m^*A)}{\sqrt{(\hbar/\tau_q)^2 + (kT)^2}}. \qquad (1)$$

To extract τ_q from the data, we have used a well-established technique that analyzes the correlation field of the data as a function of magnetic field [17]. In

Figs. 3(a)–3(d) (triangles), we demonstrate how τ_q is tuned using the four experimental parameters. Reducing T induces the rise in τ_q shown in Fig. 3(a). The saturation at low T is a common observation in semiconductor billiards [15,17] and in our experiments coincides with the condition $kT < \Delta E_S$. The saturation value of τ_q depends on A, which leads to the dependence shown in Fig. 3(b). In Fig. 3(c), τ_q decreases for larger values of n due to an increased coupling to the external environment [17]. We also find that τ_q scales with ℓ [Fig. 3(d)]. Thus, in summary, we vary Q using all four available billiard parameters: T, A, n, and ℓ. Table I shows the ranges of Q achieved. In Fig. 3(e), all of the D_F measurements from the seven different billiards are plotted against Q. In contrast to the distinct forms of the D_F variations shown in Figs. 3(a)–3(d), all of the D_F data condense onto a single "universal" curve when plotted as a function of Q. Therefore it is clear that Q is a particularly useful parameter for charting the variations in D_F. Moving from left to right across Fig. 3(e), D_F rises and then falls. This trend can be seen in the raw FCF data by moving down through Fig. 1. In the extreme limit of $Q = 0$, D_F assumes the nonfractal value of 1. As Q is increased, D_F rises smoothly until it reaches a peak value of 1.52 at $Q = 1$. Further increases in Q are accompanied by a gradual decrease in D_F. Extrapolating the downward trend in D_F, we find that to obtain $D_F = 1$ would require $Q = 11$. By this stage, the billiard width matches that of the openings and the device resembles a long quantum point contact [3].

We note that different billiard shapes and orientations of the openings were purposely used for the billiards examined (Fig. 1). Such geometric factors do not affect Q. Figure 3(e) demonstrates that these factors do not influence D_F either, further supporting our observation that Q is the relevant parameter for charting the evolution towards nonfractal behavior. In identifying Q, we emphasize that D_F is determined only by conditions *within* the billiard rather than the electron injection properties. Billiard opening parameters, such as n, only affect D_F indirectly through their effect on τ_q and therefore Q. Finally, future investigations will address the effect on D_F of varying the softness of the wall profile. Whereas the heterostructure of Fig. 1 features a single sheet of electrons (located ~70 nm below the surface), we are currently fabricating "double-layer" heterostructures that feature two parallel sheets located at different depths (~70 and ~150 nm) [18]. These investigations will use a common set of surface gates to define two nominally identical billiards which, due to their differing depths, will have different wall softness.

To conclude, we find that FCF are remarkably robust. Only in the *extreme* regimes of $Q = 0$ and $Q = 11$ do the fluctuations become nonfractal. The transition to these extremes is characterized by a smooth decrease in D_F from its peak value at $Q = 1$. This novel behavior has no simple explanation. In particular, how the suppression relates to quantum chaos [19,20] and wave-function scarring [21,22] presents a new challenge to both experimentalists and theorists.

We thank M. Pepper (Cambridge University, U.K.), C. P. Dettmann (Bristol University, U.K.), D. K. Ferry (Arizona State University, U.S.A.), C. R. Tench (University of Nottingham, U.K.), and R. Haydock (University of Oregon, U.S.A.) for valuable discussions.

*Corresponding author.
Email address: rpt@darkwing.uoregon.edu

[1] B. B. Mandelbrot, *The Fractal Geometry of Nature* (Freeman, New York, 1977).
[2] J.-F. Gouyet, *Physics and Fractal Structures* (Springer-Verlag, New York, 1996).
[3] C. W. J. Beenakker and H. van Houten, Solid State Phys. **44**, 1 (1991).
[4] T. M. Fromhold, C. R. Tench, R. P. Taylor, A. P. Micolich, and R. Newbury, Physica (Amsterdam) **249B–251B**, 334 (1998).
[5] R. Ketzmerick, Phys. Rev. B **54**, 10 841 (1996).
[6] Y. Takagaki and K. H. Ploog, Phys. Rev. B **61**, 4457 (2000).
[7] E. Louis and J. A. Vergés, Phys. Rev. B **61**, 13 014 (2000).
[8] R. A. Jalabert, H. U. Baranger, and A. D. Stone, Phys. Rev. Lett. **65**, 2442 (1990).
[9] R. P. Taylor *et al.,* Phys. Rev. Lett. **78**, 1952 (1997).
[10] A. P. Micolich *et al.,* J. Phys. Condens. Matter **10**, 1339 (1998).
[11] A. S. Sachrajda *et al.,* Phys. Rev. Lett. **80**, 1948 (1998).
[12] R. P. Taylor, Nanotechnology **5**, 183 (1994).
[13] B. Dubuc, J.-F. Quiniou, C. Roques-Carmes, C. Tricot, and S. W. Zucker, Phys. Rev. A **39**, 1500 (1989).
[14] For example, transitions towards either the fully classical regime (induced by reducing the phase coherence time) or the fully quantum-mechanical regime (induced by reducing A and therefore the Heisenberg time $\hbar/\Delta E_S$, where ΔE_S is the billiard's average energy level spacing) have been predicted to shift the lower cutoff to higher field scales, thus reducing the observation range [11].
[15] R. M. Clarke *et al.,* Phys. Rev. B **52**, 2656 (1995).
[16] Guided by the Boltzmann picture of conductance, we determine ΔE_B from a convolution of the two energy broadening distributions—the scattering-broadened density of states and the derivative of the Fermi-Dirac function [J. M. Ziman, *Electrons and Phonons: The Theory of Transport Phenomena in Solids* (Clarendon Press, Oxford, 1960)]. We find that, for the parameter ranges considered, ΔE_B can be most closely approximated by the quadrature summation of the two characteristic widths kT and $\hbar/\tau_q$.
[17] J. P. Bird *et al.,* Surf. Sci. **361/362**, 730 (1996).
[18] E. H. Linfield, G. A. C. Jones, D. A. Ritchie, and J. H. Thompson, Semicond. Sci. Technol. **8**, 415 (1993).
[19] For a review, see K. Nakamura, *Quantum Chaos—A New Paradigm of Non-linear Dynamics* (Cambridge University Press, Cambridge, 1993).
[20] K.-F. Berggren and Z.-L. Ji, Chaos **6**, 543 (1996).
[21] E. J. Heller, Phys. Rev. Lett. **53**, 1515 (1984).
[22] J. P. Bird *et al.,* Phys. Rev. Lett. **82**, 4691 (1999).